Decoupled Modeling and Nonlinear Speed Control for Five-Phase PM Motor Under Single-Phase Open Fault

Bing Tian, Qun-Tao An, *Member, IEEE*, Jian-Dong Duan, Dong-Yang Sun, Li Sun, *Member, IEEE*, and Dmitry Semenov

***Abstract*—Fault-tolerant control of a five-phase (5Ph) permanent magnet (PM) motor has been recently widely studied, however decoupled modeling under faulty conditions is discussed in less details. In this paper, decoupled model of the 5Ph PM motor under single-phase open fault is investigated and based on the proposed model field oriented control (FOC) is applied to the motor. The proposed model is based on the concept of preserving values of fundamental magnetic motive force (MMF) and back electromotive force (EMF) under single-phase open fault, the same as in healthy case, along with keeping equal torque equation at fundamental rotating space. Nevertheless, the output torque still presents some noises due to third harmonics of air-gap flux and system uncertainties, and to cope with those disturbances, sliding mode control (SMC) is proposed in the speed loop to improve the speed performance. The proposed SMC contains a PI controller and a chattering term, and thus it can be easily tuned. The decoupled model is verified by transient finite element analysis finite element analysis (FEA) and further experiment results are presented to confirm the effectiveness of the proposed control strategy.**

***Index Terms*—Adaptive sliding mode control (SMC), decoupled model, five-phase PM motor, postfault control.**

I. Introduction

FAULT-TOLERANT capacity is one of the most outstanding features of five-phase (5Ph) permanent magnet (PM) motors. It increases reliability of 5Ph drive and guarantees safe operation, and hence attracts great attention. In comparison with conventional three-phase (3Ph) PM motors, 5Ph machines exhibit a higher phase redundancy and even after failures of one or more phases the faulty machine can still continue to operate [1], [2]. Among the most common type of faults is the open circuit fault, which occurs between the machine and inverter power supply, and many articles on fault-tolerant control have been published in this field. In fault-tolerant control, remaining phase currents have to be rearranged and adapted for open circuit conditions [3]–[7]. In most of the related literatures the postfault current reconfiguration is based on criteria of preserving undisturbed rotating magnetic motive force (MMF) as in the normal operation [4], [5]. The postfault current reconfiguration problem is a multiple-solution problem, but the unique solution (or optimal solution) can be found by applying additional constraints such as: minimizing overall joule losses, keeping balanced phase currents, and minimizing postfault torque ripples [7]–[9]. The reconfiguration of phase currents can also be done in other different ways. In [10] mirror symmetry of healthy phases with respect to the faulty phase is proposed to rearrange postfault currents while keeping fundamental power constant. In [11], the same approach as previously [10] is extended to a pentagon-connection motor, and the output torque is improved by a zero-sequence current; however, additional hardware connections are required for the sake of controlling the zero-sequence current. Arafat and Seungdeog [12] present an advance vector control method to maximize the postfault torque with the aid of reluctance torque, but the optimal current solution varies with load conditions. Consequently, published articles focus on how to improve the postfault torque by the injection of third harmonic currents and similar torque behaviors are given. Also notice that most of above methods for the calculation of postfault currents are motor parameter dependent and only off-line solutions are presented. For the purpose of calculating postfault currents in real time, a vectorial approach is developed in [13], however the computation is still complex especially when taking into account a machine with trapezoidal back-electromotive forces (EMFs).

It should be emphasized that most methods for calculating optimum current references are performed at phase coordinate, thus only hysteresis current control can be applied for the perfect tracking performance of ac signals [8], [14], [15]. However, hysteresis control is not a desirable approach for high-power application due to problems associated with inconstant switching frequency [16]. For most industry applications field oriented control (FOC) with synchronous frame PI controllers is more attractive [17].

FOC is an effective motor control method that turns the rotor position coupled motor model into a simple system. With FOC phase currents can be decoupled into, respectively, flux-generation and torque-generation components. Then the torque

Manuscript received April 7, 2016; revised June 5, 2016 and August 15, 2016; accepted September 16, 2016. Date of publication September 21, 2016; date of current version February 27, 2017. This work was supported in part by the National Natural Science Foundation of China under Grants 51207029 and 51507039, in part by the Fundamental Research Funds for the Central Universities, China under Grant HIT.NSRIF.2017013, and in part by the China Postdoctoral Science Foundation under Grant 2016M591529. Recommended for publication by Associate Editor Y. Sozer.

The authors are with the Department of Electrical Engineering, Harbin Institute of Technology, Harbin, Heilongjiang 150001, China (e-mail: tianbing_hit@163.com; anquntao@163.com; duanjiandong@hit.edu.cn; 373156308@qq.com; motor611@sina.com; web24@bk.ru).

Color versions of one or more of the figures in this paper are available online at http://ieeexplore.ieee.org.

Digital Object Identifier 10.1109/TPEL.2016.2611532

and flux are independently controlled like a separately excited dc motor. FOC of 5Ph motors in normal operation has been successfully implemented [8], [18]. As for the implementation of FOC in postfault operation, two categories of methods exist. In the first case, FOC in normal operation is still considered to be applicable under faulty conditions, where failure phases are treated as a disturbance. Based on above principle, faulty motors are controlled in an intelligent manner [19], [20]. On the other hand, a new transformation of the faulty motor model into synchronous frame is performed. In [17], a postfault model at a synchronous frame is proposed for postfault operation of 5Ph PM motors. Based on this model, FOC with synchronous frame PI controllers is possible for 5Ph PM motor drive. However, coefficients of presented model are time variant, thus performance of current PI controllers will be degraded and its application is also restricted. In [7], FOC of a 5Ph induction motor under open fault is carried out basing on a set of reduced order Clarke and Park transformations. But detailed formation of the postfault motor model has not been presented. Clearly, fault-tolerant control at synchronous frame is attractive for 5Ph PMSM drive, but up to the present time no decoupled model with time-invariant coefficients is presented. In this paper, a decoupled model under open fault is proposed, thus FOC- and carrier-based PWM can be utilized for the 5Ph PM motor drive and this is one of main contributions.

It has been shown in related literatures that the postfault torque cannot be maintained as constant as in normal operation [13], [21], [22]. The ripples of the postfault torque can be resulted by third air-gap flux. But some other factors also cause torque oscillations like shaft misalignments and system uncertainties. Due to those facts the smooth control of rotor speed becomes difficult. Conventional methods are focused on the improvement of the speed by suppressing torque ripples with harmonic current injections. However, those approaches can only be completed if a high accurate postfault torque model with all uncertainties predicted and high-resolution transducers are possessed. Hence mentioned above methods are difficult to be implemented on a practical 5Ph drive. Because of the excellent disturbance rejection, nonlinear speed controls have been widely used in 3Ph drive [23], [24]. But papers focused on nonlinear speed controls in a postfault operation of 5Ph drive are rare. To suppress high uncertainties of a practical drive and improve the speed output, nonlinear controls should be developed under motor faulty conditions. Of many nonlinear controllers, sliding mode control (SMC) stands out due to ease of implementation and insensitiveness to system disturbances, thus it is quite suitable in the motor postfault operation.

SMC is introduced to overcome system uncertainties by altering the system dynamics with a discontinuous control structure [25]. The system uncertainties can be external load disturbances, unknown parameters, and system nonlinearity. The design procedure of SMC has been sufficiently detailed in [26] with a state space method. With an SMC the modeling error, which is usually stemmed from the linearization of nonlinear system, can be compensated at the expense of system chattering. In order to improve the dynamic performance of an SMC, many methods have been attempted that can be classified into: First, adopting advanced reaching laws, which are nonlinear functions of tracking error, to restrict chattering level; second, developing an adaption law to estimate system uncertainties. The latter is usually available in the control of highly nonlinear mechanical system [27], [28]. In [27], SMC with a Fuzzy logic adaption is developed for an underactuated mechanical system. This intelligent adaption law leaves some issues to be used in a real-time control system like motor drive. In [28], the backing stepping technique based on a new adaption law is proposed to estimate unknown parameters for a nonlinear hydraulic-mechanical system, and prescribed goals are reported to be achieved. This method is applied to a linear induction motor for position tracking and uncertainties occurred in the motor drive are compensated [29]. More recently a SMC-based disturbance observer is developed to compensate uncertainties in the speed tracking [30], and speed dynamics is improved. However, the structure of this SMC is complex and it is not suitable in the application of a multiphase motor drive. This paper focuses on controlling the rotor speed in a simple and effective manner, and it is of great importance for steady smooth running of the 5Ph motor under faulty conditions.

In this paper, a decoupled model of 5Ph PM motors under single-phase open circuit is proposed, and then based on this model FOC and SMC in the speed loop are further investigated. The decoupled modeling of faulty motors is based on concepts of preserving values of both fundamental MMF and back-electromotive force (EMF) the same as in normal operation and a set of reduced order Clarke and Park transformations is derived for this purpose. Consequently, voltage and torque equations at synchronous frame are formulated and they remain similar to those in normal operation. Thus, FOC and CPWM can be performed in postfault operation successfully. However, if fundamental MMF and back-EMF are preserved, third space air-gap flux will result in torque ripples. And to improve the motor speed performance an adaptive SMC is proposed. It includes a PI controller and a chattering term (shown as a sign or saturation function), and it is quite simple in structure thus can be easily implemented.

Improvements of the faulty motor drive are:

1) A decoupled model of the 5Ph motor under a single-phase open circuit is proposed. Compared to previous works, merits of this model are:
   a) it is simple and flexible to perform real-time calculation of postfault currents at synchronous frame;
   b) FOC is feasible with CPWM modulation in the postfault operation;
   c) based on this decoupled model, some advanced control methods have a potential to be applied, e.g., sensorless control of the 5Ph PM motor in the postfault operation.
2) A simple and effective adaptive SMC is also developed for the smooth running of the faulty motor. It shows a good speed dynamics and steady-state behaviors, and has a potential to replace the PI controller in the application of a slow time-variant system.

The organization of this paper is as follows. The decoupled modeling is detailed in Section II, and an adaptive SMC based on the Lyapunov function method is developed in Section III. Then

the decoupled model is verified by finite element analysis (FEA) in Section IV. Finally experimental results are provided as a confirmation of effectiveness of the proposed postfault control.

II. Proposed Decoupled Modeling Under Single-Phase Failure

The rotor type of studied motor can be as well as a surface or interior one, which is fed by a 5Ph half-bridge power inverter. The choice of faulty phases could be arbitrary, and we assume that the open circuit fault occurs in *A*-phase. Also we assume that PM flux density is not affected by the temperature, and cogging and magnetic saturation effects.

A. Principle for Decoupled Modeling

In the presence of open circuit, the 5Ph motor turns out to be an unbalanced one. The remaining healthy phase winding distribution is unsymmetrical relative to the normal mode, thus phase currents should be rearranged to adapt for the specific faulty condition. The values of remaining phase currents should be reconfigured in an asymmetrical manner in order to keep undisturbed rotating MMF before and after the faulty condition. Nonetheless, the voltage equation of normal mode is sufficient to describe the behavior of this faulty motor, and it is shown as

$$\begin{bmatrix} u_A \\ u_B \\ u_C \\ u_D \\ u_E \end{bmatrix} = R_s \begin{bmatrix} i_A \\ i_B \\ i_C \\ i_D \\ i_E \end{bmatrix} + \frac{d}{dt}\left(\begin{bmatrix} L_{AA} & L_{AB} & L_{AC} & L_{AD} & L_{AE} \\ L_{BA} & L_{BB} & L_{BC} & L_{BD} & L_{BE} \\ L_{CA} & L_{CB} & L_{CC} & L_{CD} & L_{CE} \\ L_{DA} & L_{DB} & L_{DC} & L_{DD} & L_{DE} \\ L_{EA} & L_{EB} & L_{EC} & L_{ED} & L_{EE} \end{bmatrix} \times \begin{bmatrix} i_A \\ i_B \\ i_C \\ i_D \\ i_E \end{bmatrix} \right) + \begin{bmatrix} e_A \\ e_B \\ e_C \\ e_D \\ e_E \end{bmatrix}, \quad i_A \equiv 0 \tag{1}$$

where u_A, u_B, u_C, u_D, and u_E are motor terminal voltages, which are supplied by a voltage-fed 5Ph half-bridge inverter; and e_A, e_B, e_C, e_D, and e_E indicate back-EMFs. Elements in the main diagonal of inductance matrix represent self-inductances, whereas the off-diagonal elements are mutual inductances. Motor parameters including phase inductances and back-EMFs remain unchanged because the motor itself has not been damaged. This can be explained by recognizing that stator phase windings can always be disconnected from power supply by circuit breakers or fuses, which are designed to prevent the motor from overcurrent. Thus short circuit faults in the motor are transformed to open circuit faults [31], [32].

In the case of open fault, there is no control input to regulate faulty phases. From control viewpoint, the overall voltage equation can be reduced to 4-dimension, and it is given by

$$\begin{bmatrix} u_B \\ u_C \\ u_D \\ u_E \end{bmatrix} = R_s \begin{bmatrix} i_B \\ i_C \\ i_D \\ i_E \end{bmatrix} + \frac{d}{dt}\left(\begin{bmatrix} L_{BB} & L_{BC} & L_{BD} & L_{BE} \\ L_{CB} & L_{CC} & L_{CD} & L_{CE} \\ L_{DB} & L_{DC} & L_{DD} & L_{DE} \\ L_{EB} & L_{EC} & L_{ED} & L_{EE} \end{bmatrix} \times \begin{bmatrix} i_B \\ i_C \\ i_D \\ i_E \end{bmatrix} \right) + \begin{bmatrix} e_B \\ e_C \\ e_D \\ e_E \end{bmatrix}. \tag{2}$$

In normal operation, the motor model at phase coordinate is usually decomposed into two orthogonal subspaces, i.e., fundamental rotating space and third times rotating space, with extended Clarke and Park transformations [18], [33]. However, in the presence of open faults, the symmetry property of the synchronous frame motor model is vanished. For the implementation of FOC under faulty conditions, a new set of Clarke and Park transformations should be developed. In this paper, the decoupled modeling of a faulty motor is based on the concept of maintaining fundamental MMF and back-EMF the same as in normal operation, and it is described as follows.

Since fundamental MMF is preserved equal to normal mode, for disturbance-free operation the postfault currents can be reconfigured by [8]

$$F = \frac{5}{2} N I e^{\mathrm{j}(\theta + (\pi/2))} = N(i_A + \gamma i_B + \gamma^2 i_C + \gamma^3 i_D + \gamma^4 i_E), \quad i_A \equiv 0 \tag{3}$$

where F represents fundamental MMF; N is winding turns number; I is the magnitude of fundamental excitation current; $\gamma = e^{j\delta}$, and δ is the spatial shifting angle between adjacent phases, being $\delta = 2\pi/5$; θ denotes the rotor electrical position; and i_A, i_B, i_C, i_D, and i_E are phase currents, respectively.

Based on the above principle, it is impossible to maintain equal third space MMF, and third space currents at α–β plane can be calculated by

$$i_A + \gamma^3 i_B + \gamma^6 i_C + \gamma^9 i_D + \gamma^{12} i_E = i_{a3} + \mathrm{j}\, i_{\beta 3},\ i_A \equiv 0 \tag{4}$$

where $i_{\alpha 3}$ and $i_{\beta 3}$ are third space currents at α–β plane.

In consideration of the zero-sequence current, which is constraining to zero because of stator winding star connections, (3) and (4) can be synthesized as

$$\frac{2}{5} \begin{bmatrix} \cos\delta & \cos 2\delta & \cos 2\delta & \cos\delta \\ \sin\delta & \sin 2\delta & -\sin 2\delta & -\sin\delta \\ \cos 2\delta & \cos\delta & \cos\delta & \cos 2\delta \\ -\sin 2\delta & \sin\delta & -\sin\delta & \sin 2\delta \\ 1 & 1 & 1 & 1 \end{bmatrix} \begin{bmatrix} i_B \\ i_C \\ i_D \\ i_E \end{bmatrix} = \begin{bmatrix} i_\alpha \\ i_\beta \\ i_{\alpha 3} \\ i_{\beta 3} \\ 0 \end{bmatrix} \tag{5}$$

where i_α and i_β are the fundamental space currents at α--β plane, respectively. In this paper, star winding connection is preferable due to the absence of zero-sequence current, and the rule of (5) can never be applied to motors with open-type windings.

Since the third row vector in (5) is not orthogonal with other vectors, by removing the third line and correcting the first row

vector with zero-sequence current, one can obtain

$$\frac{2}{5}\begin{bmatrix}\cos\delta+x & \cos2\delta+x & \cos2\delta+x & \cos\delta+x\\ \sin\delta & \sin2\delta & -\sin2\delta & -\sin\delta\\ -\sin2\delta & \sin\delta & -\sin\delta & \sin2\delta\\ 1 & 1 & 1 & 1\end{bmatrix}\times\begin{bmatrix}i_B\\ i_C\\ i_D\\ i_E\end{bmatrix}=\begin{bmatrix}i_\alpha\\ i_\beta\\ i_3\\ 0\end{bmatrix} \tag{6}$$

where i_3 represents the third space current; x is the correction factor. It should be noted that the equality of the first row still holds because of no zero-sequence current.

For the postfault operation, the trajectory of back-EMFs of healthy phases should also form a circle, and the correction factor x in (6) is selected for above purpose. Thus, we define a reduced order Clarke transformation as

$$[\mathbf{T}_{\text{clark}}]=\frac{2}{5}\begin{bmatrix}\cos\delta+x & \cos2\delta+x & \cos2\delta+x & \cos\delta+x\\ \sin\delta & \sin2\delta & -\sin2\delta & -\sin\delta\\ -\sin2\delta & \sin\delta & -\sin\delta & \sin2\delta\\ 1 & 1 & 1 & 1\end{bmatrix}. \tag{7}$$

Projecting back-EMFs of remaining phases to α–β plane with this new Clarke transformation, it yields

$$\begin{aligned}E_\alpha &= \cos\delta E_b+\cos2\delta E_c+\cos2\delta E_d+\cos\delta E_e\\ &\quad -x(E_b+E_c+E_d+E_e)\\ &= xE_a+\cos\delta E_b+\cos2\delta E_c+\cos2\delta E_d+\cos\delta E_e \quad (8)\\ E_\beta &= 0E_a+\sin\delta E_b+\sin2\delta E_c-\sin2\delta E_d-\sin\delta E_e \quad (9)\end{aligned}$$

where E_α and E_β are back-EMFs of α–β frame; and E_a, E_b, E_c, E_d, and E_e are back-EMFs at the natural reference frame.

As can be seen from (8) and (9), when x in (7) is not properly selected, back-EMFs of remaining phases at α–β plane cannot form a circle. This means electromagnetic energy conversion of the faulty motor is unstable. Because of $E_a+E_b+E_c+E_d+E_e=0$, the trajectory of E_α and E_β under faulty conditions can form a circle by letting $x=-1$. Thus, circle rotation of remaining phase back-EMFs is achieved and kept the same as in the normal mode.

To simplify the decoupled modeling, we use the following to represent the voltage equation of the 5Ph motor under faulty conditions

$$[\mathbf{U}_s]=R_s[\mathbf{I}_s]+\frac{d}{dt}([\mathbf{L}_s][\mathbf{I}_s]+[\psi_{m-s}]) \tag{10}$$

where $[\mathbf{U}_s]$ denotes the phase-voltage vector, $[\mathbf{I}_s]$ is the phase-current vector, $[\mathbf{L}_s]$ indicates phase-inductance matrix; $[\psi_{m-s}]$ represents the vector of PM-flux linkage; and R_s the stator resistance. The subscript "s" means that (10) is established at the natural reference frame. Hereafter, (10) indicates a reduced order voltage equation where A-phase related quantities have been removed due to the absence of current. Then with a reduced order Park transformation, as shown in (11), the faulty motor model can be transformed into synchronous frame (d–q–3–o frame)

$$[\mathbf{T}_{\text{park}}]=\begin{bmatrix}\cos\theta & \sin\theta & 0 & 0\\ -\sin\theta & \cos\theta & 0 & 0\\ 0 & 0 & 1 & 0\\ 0 & 0 & 0 & 1\end{bmatrix} \tag{11}$$

where $[\mathbf{T}_{\text{park}}]$ is a reduced order park transformation matrix under single-phase open fault. This rotational transformation incorporates a standard Park representation used for a 3Ph ac motor drive, as indicated in the first two rows. Thus, α–β frame components can be transformed to dc components. Since the trajectory of a third space component under open fault is unable to form a circle, this component can never be decoupled with a rotational transformation.

Therefore the motor terminal voltage equation at the d–q–3–o frame can be expressed by

$$\begin{aligned}[\mathbf{U}_{qd3o}] &= [\mathbf{T}_{\text{park}}][\mathbf{T}_{\text{clark}}][\mathbf{U}_s]\frac{\partial^2\Omega}{\partial u^2}\\ &= R_s[\mathbf{I}_{qd3o}]+[\mathbf{T}_{\text{park}}][\mathbf{T}_{\text{clark}}]\underbrace{\frac{d([\mathbf{L}_s][\mathbf{I}_s])}{dt}}_{\text{Induced EMF}}\\ &\quad +[\mathbf{T}_{\text{park}}][\mathbf{T}_{\text{clark}}]\underbrace{\frac{d[\psi_{m-s}]}{dt}}_{\text{Back EMF}}\end{aligned} \tag{12}$$

here

$$[\mathbf{U}_{dq3o}]=[\mathbf{T}_{\text{park}}][\mathbf{T}_{\text{clark}}][\mathbf{U}_s],[\mathbf{I}_{dq3o}]=[\mathbf{T}_{\text{park}}][\mathbf{T}_{\text{clark}}][\mathbf{I}_s]. \tag{13}$$

By taking a derivative of magnetic co-energy with respect to rotor electrical position (θ), one can obtain torque equation

$$T_e=\frac{\partial W_{\text{co}}}{\partial\theta}=P\left(\frac{1}{2}[\mathbf{I}_s^{\text{T}}]\frac{\partial[\mathbf{L}_s]}{\partial\theta}[\mathbf{I}_s]+[\mathbf{I}_s^{\text{T}}]\frac{\partial[\psi_{m-s}]}{\partial\theta}\right) \tag{14}$$

where W_{co} indicates magnetic co-energy. As can be seen, the precise knowledge of phase inductance is required for the postfault torque calculation. In most of related articles, the magnetic energy stored in the toroid is omitted; however, this part is important for some types of PM machines. Thus, phase inductances should be considered in the postfault torque calculation.

B. Decoupled Model Under Single-Phase Open Fault

In a 5Ph motor the windings are usually wound in a trapezoidal fashion and give a trapezoidal-shape back-EMF. According to the winding function theory this type of rectangular stator winding produces first, third, fifth, and seventh harmonic back-EMFs [17]. To simplify the postfault modeling, only the first and third harmonics are considered.

Back-EMFs are produced by magnetic flux linkages. Since A-phase is uncontrollable, we will remove A-phase related

quantities from the PM flux linkage vector [17], [18], [33]

$$[\psi_{m-s}] = \psi_{m1}\begin{bmatrix}\cos(\theta-\delta)\\ \cos(\theta-2\delta)\\ \cos(\theta-3\delta)\\ \cos(\theta-4\delta)\end{bmatrix} + \psi_{m3}\begin{bmatrix}\cos 3(\theta-\delta)\\ \cos 3(\theta-2\delta)\\ \cos 3(\theta-3\delta)\\ \cos 3(\theta-4\delta)\end{bmatrix} \tag{15}$$

where ψ_{m1} and ψ_{m3} denote ,respectively, amplitudes of first and third harmonics of PM flux linkage.

According to (12), the back-EMF at synchronous frame is

$$\begin{aligned}[\mathbf{E}_{dq3o}] &= [\mathbf{T}_{\text{park}}][\mathbf{T}_{\text{clark}}]\frac{d}{dt}[\psi_{m-s}]\\ &= \frac{d([\mathbf{T}_{\text{park}}][\mathbf{T}_{\text{clark}}][\psi_{m-s}])}{dt}\\ &\quad - \frac{d[\mathbf{T}_{\text{park}}]}{dt}[\mathbf{T}_{\text{clark}}][\psi_{m-s}]\end{aligned} \tag{16}$$

where $[\mathbf{E}_{dq3o}]$ represents back-EMF vector at the *d*–*q*–3–*o* frame.

Substitute (7), (11), and (15) into (16) one can obtain

$$[E_{dq3o}] = \begin{bmatrix}E_d\\ E_q\\ E_3\\ E_o\end{bmatrix} = \omega\psi_{m1}\begin{bmatrix}0\\ 1\\ 0\\ 0.4\sin\theta\end{bmatrix} + \omega\psi_{m3}\begin{bmatrix}0\\ 0\\ 3\cos 3\theta\\ 1.2\sin 3\theta\end{bmatrix} \tag{17}$$

where E_d, E_q, E_3, and E_o are, respectively, *d*-axis, *q*-axis, third space, and zero-sequence components of back-EMFs. As can be seen, back-EMFs of fundamental space are completely decoupled whereas third space component is pulsating. Since the reduced order Clarke transformation can only keep fundamental back-EMFs equal to normal mode, the fluctuation of back-EMF at third space is unavoidable. The back-EMF of third space (E_3) will interact with fundamental space currents, generating power ripples and this is undesirable for the postfault operation. Also it should be noted that there are no ripples in power output at zero-sequence space due to absence of the zero-sequence current.

Fundamental currents flow in stator windings, producing self-induced and mutually induced EMFs, and according to (12) those induced EMFs at synchronous frame can be expressed by

$$\begin{aligned}\left[\mathbf{E}_{L-dq3o}\right] &= [\mathbf{T}_{\text{park}}][\mathbf{T}_{\text{clark}}]\frac{d([\mathbf{L}_s][\mathbf{I}_s])}{dt}\\ &= \frac{d([\mathbf{T}_{\text{park}}][\mathbf{T}_{\text{clark}}][\mathbf{L}_s][\mathbf{I}_s])}{dt}\\ &\quad - \frac{d([\mathbf{T}_{\text{park}}][\mathbf{T}_{\text{clark}}])}{dt}[\mathbf{L}_s][\mathbf{I}_s]\\ &= \frac{d[\mathbf{L}_{dq3o}]}{dt}[\mathbf{I}_{dq3o}] + [\mathbf{L}_{dq3o}]\frac{d[\mathbf{I}_{dq3o}]}{dt}\\ &\quad - [\Omega][\mathbf{L}_{dq3o}][\mathbf{I}_{dq3o}]\end{aligned} \tag{18}$$

where

$$[\mathbf{L}_{dq3o}] = [\mathbf{T}_{\text{park}}][\mathbf{T}_{\text{clark}}][\mathbf{L}_s]\left[(\mathbf{T}_{\text{clark}})^{-1}\right]\left[(\mathbf{T}_{\text{park}})^{-1}\right] \tag{19}$$

$$[\mathbf{\Omega}] = \frac{d([\mathbf{T}_{\text{park}}])}{dt}([\mathbf{T}_{\text{park}}])^{-1} = \omega\begin{bmatrix}0 & 1 & 0 & 0\\ -1 & 0 & 0 & 0\\ 0 & 0 & 0 & 0\\ 0 & 0 & 0 & 0\end{bmatrix}. \tag{20}$$

In above relationships $[\mathbf{E}_{L-dq3o}]$ indicates the induced EMF due to stator current variation; $[\Omega]$ the matrix of angular speed (electrical); and $[\mathbf{L}_{dq3o}]$ the inductance matrix of *d*–*q*–3–*o* frame. In normal operation the inductance matrix at two rotating subspaces is constant and symmetrical, thus the first term of (16) is [0], which is indicated as a time derivative of $[\mathbf{L}_{-dq3o}]$. The reduced-order Clarke transformation presented in this paper also guarantees that inductances of fundamental synchronous rotating space are constant.

According to the spectrum of winding density distribution, $[\mathbf{L}_s]$ incorporates leakage inductance quantity, zero-frequency as well as second and sixth harmonic inductance quantities. Neglecting the sixth harmonic of $[\mathbf{L}_s]$ due to its small value, inductances of remaining phases can be presented as [17], [18], and [33]

$$[\mathbf{L}_s] = L_{ls}[\mathbf{I}_4] + [\mathbf{L}_{0\theta}] - [\mathbf{L}_{2\theta}] + [\mathbf{L}_{6\theta}],\quad [\mathbf{L}_{2\theta}] \approx 0 \tag{21}$$

$$[\mathbf{L}_{0\theta}] = L_m\begin{bmatrix}1 & \cos\delta & \cos 2\delta & \cos 2\delta\\ \cos\delta & 1 & \cos\delta & \cos 2\delta\\ \cos 2\delta & \cos\delta & 1 & \cos\delta\\ \cos 2\delta & \cos 2\delta & \cos\delta & 1\end{bmatrix} \tag{22}$$

$$[\mathbf{L}_{2\theta}] = L_\theta\begin{bmatrix}\cos 2\theta_1 & \cos 2\theta_4 & \cos 2\theta_2 & \cos 2\theta_0\\ \cos 2\theta_4 & \cos 2\theta_2 & \cos 2\theta_0 & \cos 2\theta_3\\ \cos 2\theta_2 & \cos 2\theta_0 & \cos 2\theta_3 & \cos 2\theta_1\\ \cos 2\theta_0 & \cos 2\theta_3 & \cos 2\theta_1 & \cos 2\theta_4\end{bmatrix} \tag{23}$$

where L_{ls} is leakage inductance; $[\mathbf{I}_4]$ is an identity matrix of order 4; $[\mathbf{L}_{0\theta}]$ is constant inductance matrix, with L_m being its magnitude; $[\mathbf{L}_{2\theta}]$ is the second harmonic inductance matrix, which is modulated by θ, with L_θ being its magnitude; and $\theta_i = \theta - i\delta$, being $i = 0, 1, 2, 3, 4$. The motor inductance is related to a machine structure, and as previously illustrated its value is not affected by open circuit faults. In some published articles $[\mathbf{L}_{2\theta}]$ is not considered in posttorque modeling; however, this part is crucial for most machines performing advanced control (e.g., sensorless control) and thus cannot be neglected.

Substitute (7), (11), and (21) into (19) one can obtain *d*–*q* frame inductance matrix as shown in (24), where $L_d = L_{ls} + 2.5(L_m - L_\theta)$, $L_q = L_{ls} + 2.5(L_m + L_\theta)$, respectively.

As can be seen, (24) gets symmetrical when all of the zero-sequence related components from the fourth row and fourth column are removed. The values of L_d and L_q under open fault remain the same as in normal mode [33]. This property is important to dynamic behaviors of inner current loops, which strongly relies upon *d*–*q* frame inductances. Thus adopting such

a model frees the model-based control from determination of a new set of parameters for the postfault operation.

By ignoring the zero-sequence related quantities, substitute (7), (11), (17), and (24) into (12), the voltage equation at *d*–*q*–3, see (24) and (25) as shown at the bottom of the page, frame can be derived as shown in (25), where u_d, u_q, and u_3 are, respectively, voltage quantities of *d*-axis, *q*-axis, and third space; and i_d, i_q, and i_3 are, respectively, current quantities of *d*-axis, *q*-axis, and third space. It is interesting to see that this voltage equation at fundamental space remains the same as in normal operation. This is because values of the MMF and back-EMF of fundamental space are kept equal to normal operation ones, and it is done by utilization of reduced order Clarke transformation where $x = -1$.

From control point of view, phase currents are decoupled into three parts: a flux-generating part (i_d), a torque-generating part (i_q), and third space part (i_3), respectively. Thus this faulty motor model enables the regulation of electromagnetic torque by i_q and field weakening by i_d, and it is also possible to use synchronous frame PI controllers.

Substitute (7), (11), (15), and (21) into (14), the electromagnetic torque is obtain as

$$T_e = T_{e1} + T_{e3} \tag{26}$$

$$T_{e1} = \frac{5}{2} P i_d i_q (L_d - L_q) + \frac{5}{2} P i_q \psi_{m1} \tag{27}$$

$$T_{e3} = \frac{5}{2} P \psi_{m3} \left(3 i_3 \cos 3\theta + \frac{3\left(-i_q \cos 2\theta + i_d \sin 4\theta\right)}{2} + \frac{3\left(i_q \cos 4\theta + i_d \sin 2\theta\right)}{2} \right) \tag{28}$$

where T_e denotes overall electromagnetic torque, T_{e1} is a fundamental torque, and T_{e3} stands for ripples in the torque. As can be seen, because of preservation of fundamental MMF and back-EMFs, the fundamental torque (T_{e1}) also remains the same as in normal operation. As previously noted, the third space back-EMF is pulsating with frequency 3θ and amplitude $3\omega\psi_{m3}$. Torque ripples (T_{e3}) exist due to the fact that this pulsating back-EMF (E_3) interacts with fundamental space current as well as third space current:

$$E_3 = 3\omega\psi_{m3} \cos 3\theta = \frac{1}{2} 3\omega\psi_{m3} e^{j3\theta} + \frac{1}{2} 3\omega\psi_{m3} e^{-j3\theta}. \tag{29}$$

The pulsating back-EMF, shown as above, can be divided into two oppositely rotating vectors, i.e., positive and negative sequences, each with half the amplitude of overall pulsating back-EMF. The positive- and negative-sequence components interact with fundamental space currents, generating power oscillation at twice and four times of synchronous speed. Along with that the third space EMF also interacts with third space current, inducing extra power ripples.

The decoupled model is one of the main contributions of this paper. With this model FOC can be used for the post fault operation with a little modification to the normal mode control scheme.

III. Proposed Nonlinear Speed Control

A. FOC for PostFault Operation

According to (26), the postfault torque is determined by the fundamental torque (T_{e1}). Clearly, with $i_d = 0$ control the average torque can be determine by i_q. The third space current value (i_3) can be acquired by imposing additional constraints: phase current reconfiguration is calculated by lowest joule losses (LJL) or a equal joule losses (EJL) control criteria.

1) LJL Control Criterion: When adopting LJL criterion, current references at *d*–*q*–3 frame can be presented as

$$i_d = 0, i_q = \text{constant}, i_3 = 0. \tag{30}$$

Since the joule losses can be expressed by $R_s(i_d^2 + i_q^2 + i_3^2)$ according to (14), it is clear that minimal losses value $(R_s\, i_q^2)$ is achieved by adopting $i_d = 0$ and $i_3 = 0$ control.

By substituting constraints of $i_d = 0$ and $i_3 = 0$ into (26), the torque under LJL criterion is simplified as

$$T_e = K_{Te} i_q \left(1 - \frac{1}{2}\frac{\psi_{m3}}{\psi_{m1}} \cos 2\theta + \frac{1}{2}\frac{\psi_{m3}}{\psi_{m1}} \cos 4\theta\right),$$
$$K_{Te} = 2.5 P \psi_{m1}. \tag{31}$$

In above equation the torque constant K_{Te} is defined as $2.5P\psi_{m1}$ where the coefficient 2.5 is introduced by 5h electrical power calculation, and coefficient $1/2$ in the torque expression is a result of the separation of positive and negative sequences from the pulsating back-EMF, whose trajectory cannot be preserved as a circle at the new α–β plane due to open circuit faults.

2) EJL Control Criterion: When the EJL criterion is adopted, the current amplitude of each healthy phase is required to be kept equal. In this case, the phase current can be reconfigured by imposing extra constraints of $i_b = -i_d$ and $i_c = -i_e$ [34]. According to the principle of preservation of fundamental

$$[\mathbf{L}_{dq3o}] = \begin{bmatrix} L_d & 0 & 0 & (L_d - L_{ls})\cos\theta \\ 0 & L_q & 0 & -(L_q - L_{ls})\sin\theta \\ 0 & 0 & L_{ls} & 0 \\ -0.4(L_d - L_{ls})\cos\theta & 0.4(L_q - L_{ls})\sin\theta & 0 & 0.2(7L_{ls} - L_d - L_q - (L_d - L_q)\cos 2\theta) \end{bmatrix} \tag{24}$$

$$\begin{bmatrix} u_d \\ u_q \\ u_3 \end{bmatrix} = R_s \begin{bmatrix} i_d \\ i_q \\ i_3 \end{bmatrix} + \begin{bmatrix} L_d & 0 & 0 \\ 0 & L_q & 0 \\ 0 & 0 & L_{ls} \end{bmatrix} \frac{d}{dt} \begin{bmatrix} i_d \\ i_q \\ i_3 \end{bmatrix} - \omega \begin{bmatrix} 0 & L_q & 0 \\ -L_d & 0 & 0 \\ 0 & 0 & 0 \end{bmatrix} \begin{bmatrix} i_d \\ i_q \\ i_3 \end{bmatrix} + \omega \begin{bmatrix} 0 \\ \psi_{m1} \\ 3\psi_{m3}\cos 3\theta \end{bmatrix} \tag{25}$$

TABLE I
PREFERENCES OF THE REQUIRED JOULE LOSS CONTROL CRITERION

Lowest Joule Losses	Equal Joule Losses
$a = 1.5\psi_{m\,3}/\psi_{m\,1}$	$a = 1.146\psi_{m\,3}/\psi_{m\,1}$
$b = 1.5\psi_{m\,3}/\psi_{m\,1}$	$b = 1.854\psi_{m\,3}/\psi_{m\,1}$

MMF, we can obtain the following relationship from (6)

$$\begin{aligned} i_\beta &= \sin\delta i_b + \sin 2\delta i_c - \sin 2\delta i_d - \sin\delta i_e \\ &= (i_b + i_c)(\sin\delta + \sin 2\delta) \end{aligned} \tag{32}$$

$$\begin{aligned} i_3 &= -\sin 2\delta i_b + \sin\delta i_c - \sin\delta i_d - \sin 2\delta i_e \\ &= \frac{\sin\delta - \sin 2\delta}{\sin\delta + \sin 2\delta} i_\beta = 0.236 i_q \cos\theta \end{aligned} \tag{33}$$

where $\frac{\sin\delta - \sin 2\delta}{\sin\delta + \sin 2\delta} = 0.236$.

Thus we can obtain optimal postfault currents of *d–q* frame for the purpose of EJL control, and it is given by

$$i_d = 0, i_q = \text{constant}, i_3 = 0.236 i_q \cos\theta \tag{34}$$

Then substitute (34) into overall torque equation (26) as

$$T_e = K_{Te} i_q \left(1 - \frac{1.146\psi_{m3}}{\psi_{m1}} \cos 2\theta + \frac{1.854\psi_{m3}}{\psi_{m1}} \cos 4\theta\right) \tag{35}$$

where $1.146 = \frac{3}{2}(1 - \frac{\sin\delta - \sin 2\delta}{\sin\delta + \sin 2\delta})$ $1.854 = \frac{3}{2}(1 + \frac{\sin\delta - \sin 2\delta}{\sin\delta + \sin 2\delta})$.

Therefore a generalized torque equation can be expressed as follows, considering above criteria for joule losses control:

$$T_e = K_{Te} i_q (1 - a\cos 2\theta + b\cos 4\theta) \tag{36}$$

where a and b are defined as harmonic factors, and they are shown in Table I.

As can be seen, with $i_d = 0$ control the torque behavior is nonlinear, and torque ripples concentrates mainly on the frequency that is twice and four times of synchronous speed. Clearly amplitudes of harmonics are related to ψ_{m3}/ψ_{m1}, thus motors with sinusoidally distributed winding are more appropriate for torque ripple free applications, due to $\psi_{m3} = 0$. However, the studied motor has trapezoidal-shape back-EMFs, and it is impossible to alter the stator winding configuration. Torque ripples result in a fluctuation of the rotor speed, which means if speed curve is smooth, then the electromagnetic torque is also thought to be constant. From control point of view, nonlinear speed control should be developed to suppress unpredicted and unmodeled dynamics of a real drive.

B. Nonlinear Speed Control

Commonly, the torque command is generated by the speed PI controller. It is general knowledge that the PI controller cannot deal with problems associated with nonlinear system [28], [30], and thus we utilized SMC to tackle this issue.

Motion equation of 5Ph drive is expressed as

$$\begin{cases} \dot\theta = \omega \\ \dot\omega = (P/J)T_e - (P/J)T_L + D(t) \end{cases} \tag{37}$$

where J is the measured value of rotational inertia constant, T_e represents the control input; T_L indicates the load torque; and $D(t)$ denotes the lumped disturbance, which is formulated as

$$D(t) = -B_m\omega(P/J) + f(\Delta J, \Delta B_m) + f_{\text{unknown}}(t) \tag{38}$$

where B_m represents measured value of viscous friction coefficient; $f(\Delta J, \Delta B_m)$ indicates the mismatch between the measured parameters and real values; and $f_{\text{unknown}}(t)$ denotes time-variant disturbances that can be traced to the cogging effect, magnetic saturation effect, nonlinearity of voltage source inverter, etc. D(t) is assumped to be bound as

$$\max(|D(t)|) < K \tag{39}$$

where K is a positive constant.

Define the sliding surface as

$$s = c\,e = c\,(\omega_{\text{ref}} - \omega) \tag{40}$$

where e is the angular speed tracking error; subscript "ref" means the corresponding variable is a reference; and c is a positive constant that guarantees the system state error is driven to the sliding surface at finite time. The state error always moves from an initial condition to the sliding surface $s = 0$ and stay on it if $s\dot s < 0$.

The control strategy of SMC is to find a control law such that the angular speed can track the reference. The control law is based on the Lyapunov function method, and it incorporates T_L, which is however difficult to be measured precisely. In this paper, T_L is updated by an adaptive algorithm that is described as the following.

Define estimated error of load torque as

$$\Delta T_L = T_L - \widehat{T}_L \tag{41}$$

where $\widehat{T}_L$ is estimated value of the load torque and ΔT_L is the estimated error.

Define the Lyapunov function as

$$V = \frac{1}{2}s^2 + \frac{1}{2\lambda}\Delta T_L^2, \quad \lambda > 0 \tag{42}$$

where λ represent the adaption gain.

To force e and ΔT_L converge to zero, the derivative of V must satisfy the requirement of less than zero:

$$\begin{aligned} \dot V &= s\dot s + \frac{\Delta T_L(\dot T_L - \dot{\widehat{T}}_L)}{\lambda} = c^2 e\dot e - \frac{\Delta T_L \dot{\widehat{T}}_L}{\lambda} \\ &= c^2 e\left(-\frac{PT_e}{J} + \frac{P\widehat{T}}{J_L} - D(t) + \frac{P\Delta T_L}{J}\left(1 - \frac{J\dot{\widehat{T}}_L}{\lambda P c^2 e}\right)\right). \end{aligned} \tag{43}$$

In above relationship, the time derivative of T_L is assumed to be zero. This is because the sampling period of adaptive approach is much smaller than variations of the kinetic noise which is viewed as a constant during the sampling period.

The derivative of angular speed tracking error (e) is given by

$$\dot e = (\dot\omega_{\text{ref}} - \dot\omega) = -\frac{P}{J}T_e + \frac{P}{J}T_L - D(t). \tag{44}$$

Thus the control law can be obtained by letting $\dot{V} < 0$, and it is given by

$$-\frac{P}{J}T_e + \frac{P}{J}\widehat{T}_L = -K_1 e - K_2 \text{sign}(e), \quad K_1 > 0, \quad K_2 > K \tag{45}$$

where K_1 represents state feedback gain; K_2 denotes chattering boundary level; and sign $(\cdot)$ represents a sign function.

In this paper, we use an adaptive approach to estimate the value of T_L and it is shown as

$$\dot{\widehat{T}}_L = \frac{P\lambda c^2}{J} e. \tag{46}$$

Then substituting control law (T_e) and adaptive law $(\widehat{T}_L)$ into (43) yields

$$\dot{V} = -K_1 c^2 e^2 - ce\left[K_2 \text{sign}(e) + D(t)\right] < 0. \tag{47}$$

According to (47), asymptotic stability of a controlled system is guaranteed in the presence of system uncertainties and it also means that both of measured angular speed and estimated load torque converge to their respective reference or real values.

In the above relationship, one should notice that a high value of K_2 increases system chattering, but this can be partly improved by employing a saturation function instead of a sign function.

Thus the control law T_e can be designed as follows:

$$T_e = \underbrace{\frac{JK_1}{P}e + \frac{\lambda P c^2}{J}\int e}_{\text{PI Control}} + \underbrace{\frac{JK_2}{P}\text{sat}(e)}_{\text{chattering}}. \tag{48}$$

As can be seen, the first two terms of (48) represents a PI controller, which already contains the estimation of load torque. The last term of (48) corresponds to system chattering that is utilized to suppress uncertainties and disturbances. By including a simple chattering term on the basis of PI controllers, the speed performance gets enhanced with this new controller. The proposed method is also easy to implement and can guarantee a smooth running even in the presence of noises. The system chattering can be reduced by development of an advanced reaching law instead of a saturation function. However, it will cost additional multiplications in a digital signal controller (DSC) and is not considered in this paper.

Substitute (36) into (48), one can obtained

$$i_q^* = \frac{\frac{JK_1}{PK_{Te}}e + \frac{P\lambda c^2}{JK_{Te}}\int e + \frac{JK_2}{PK_{Te}}sat(e)}{(1 - a\cos 2\theta + b\cos 4\theta)} \tag{49}$$

where i_q^* is the q-axis current reference.

Fig. 1 shows the block diagram for proposed nonlinear speed controller. The coefficients that are required to be tuned include K_1, K_2, c, and λ. Of these coefficients K_1 is correlated to the convergence rate of angular speed tracking error, whereas K_2 is related to the system noise grade, including external load disturbances and parameter perturbations. A larger c in the PI controller can guarantee a smaller static tracking error of angular speed, and a smaller λ ensures a smaller estimated error of load torque. Along with that, $c\lambda$ together determines the estimation rate of load torque and the larger value always accelerates its convergence.

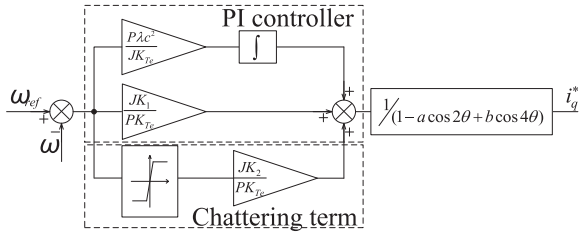

Fig. 1. Block diagram for proposed SMC.

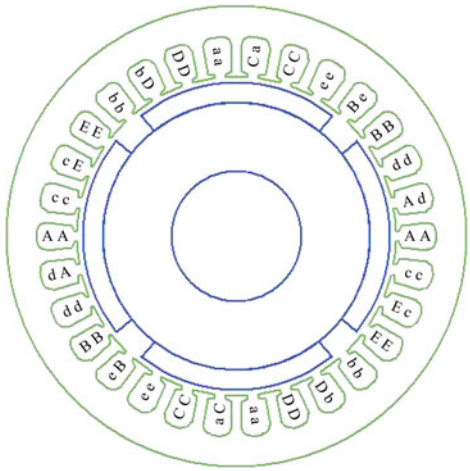

Fig. 2. Cross section of studied 5Ph PM motor.

IV. Fault-Mode Model Verification by FEA

To verify proposed decoupled model 2-D FEA is carried out based on the Ansoft/Maxwell software. Fig. 2 shows a cross section of the 5Ph surface PM motor with double-layer fractional-slot winding configuration. The parameters of this prototype motor are listed in Table II. Accuracy of proposed decoupled model is verified under the LJL and EJL control criteria.

A. Preservation of Fundamental Back-EMFs

Studied motor gives a trapezoidal-shape back-EMFs that mainly contain first and third harmonic components. Fig. 3 shows back-EMFs of A-phase and α–β frame, respectively. As can be seen with proposed Clarke transformation, first harmonics are preserved the same as these are in normal operation.

B. Verification of Decoupled Model Under LJL Criterion

To verify the accuracy of proposed model, remaining four phases are excited with $i_q = 2$ A under the LJL criterion. The torque-position characteristic by FEA is depicted in Fig. 4.

As can be seen from Fig. 4, the motor under single-phase open circuit continues to operate, but with fluctuations in the profile of output torque. Harmonic components of this torque

TABLE II
PARAMETERS OF PROTOTYPE MOTOR

Symbol	Description	Quantity
	Stator inner diameter	146 mm
	Stator outer diameter	210 mm
	Length of stator iron	65 mm
	Air gap length	3 mm
	Rotor outer diameter	140 mm
	Magnet Materials	NdFeB
	Magnet Thickness	8 mm
ψ_{m1}	Fundamental PM flux linkage	0.5154825 Wb
ψ_{m3}	Third harmonic PM flux linkage	0.024718 Wb
L_d	d-axis inductance	7.34 mH
L_q	q-axis inductance	9.18 mH
L_{ls}	Leakage inductance	1.74 mH
P	Pole pairs	2
R_s	Stator resistance (100°)	1.1 Ω
	Number of Slots	30
	Rated Phase voltage	100 V
	Rated Speed	900 r/min

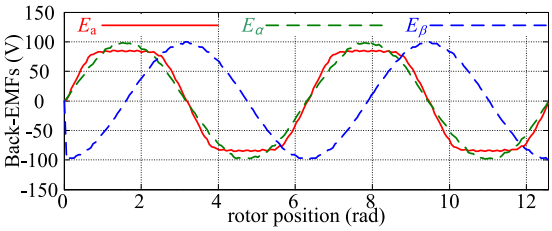

Fig. 3. Back-EMFs of A-phase and α–β frame under single-phase open fault.

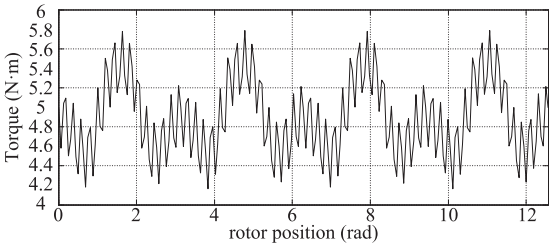

Fig. 4. Torque-position (electrical) characteristic under the LJL criterion.

TABLE III
HARMONIC CONTENTS OF OUTPUT TORQUE UNDER THE LJL CRITERION

Description	Value
Fundamental Torque	5.12248 N·m
2nd harmonic torque	0.37514 N·m
4th harmonic torque	0.39588 N·m
30th harmonic torque	0.36898 N·m

are listed in Table III, and comparisons with analytical solutions are performed as below.

According to (36), the fundamental torque is 5.154 N·m, whereas in the simulation this quantity is 5.12248 N·m. The discrepancy of these two results is 0.0312 N·m and the value of fundamental torque can be kept the same as in normal mode.

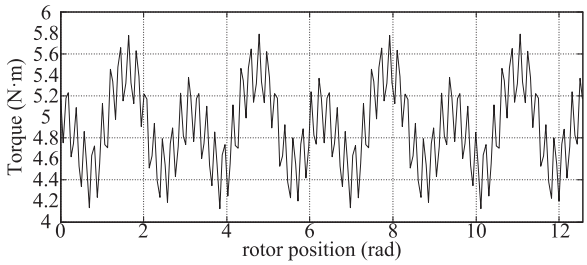

Fig. 5. Torque-position characteristic by FEA under the EJL criteria.

TABLE IV
HARMONIC CONTENTS OF THE OUTPUT TORQUE EJL CRITERION

Description	Quantity
Fundamental Torque	5.12248 N·m
2nd harmonic torque	0.28024 N·m
4th harmonic torque	0.48841 N·m
30th harmonic torque	0.36898 N·m

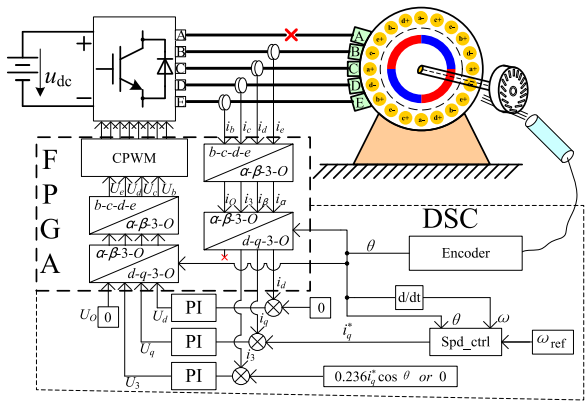

Fig. 6. Overall control scheme under single-phase open circuit fault.

The second harmonic torque is 0.3708 N·m by (36) versus 0.37512 N·m by FEA, and the fourth harmonic presents 0.3708 N·m by (36) versus 0.39588 N·m by FEA. The second and fourth harmonics by FEA are consistent with solutions of (36).

The 30th harmonic is resulted from cogging effect and this is one of the system uncertainties. In addition, the saturation effect also results in the difference between FEA and analytical results.

Clearly, the behavior of output torque by (36) remains close to that by FEA and this confirms the accuracy of the proposed decoupled model.

C. Verification of Decoupled Model Under the EJL Criterion

Further to investigate proposed decoupled model, currents under the EJL criterion are applied to the motor where i_q is still equal to 2A.

The torque-position characteristic and harmonic contents of output torque are shown in Fig. 5 and Table IV, respectively. As can be seen, the fundamental torque by FEA is 5.12852 N·m, and second and fourth harmonics are 0.28024

TABLE V
PRACTICAL PARAMETERS OF PROTOTYPE MOTOR

Symbol	Description	Quantity
ψ_{m1}	Fundamental PM flux linkage	0.535872 Wb
ψ_{m3}	Third harmonic PM flux linkage	0.033492 Wb
L_d	d-axis inductance	6.54 mH
L_q	q-axis inductance	8.32 mH
R_s	Stator resistance	1.1 Ω
	Rated speed	600 r/min

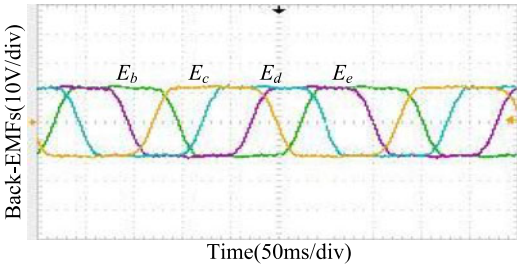

Fig. 7. Back-EMFs of healthy phases.

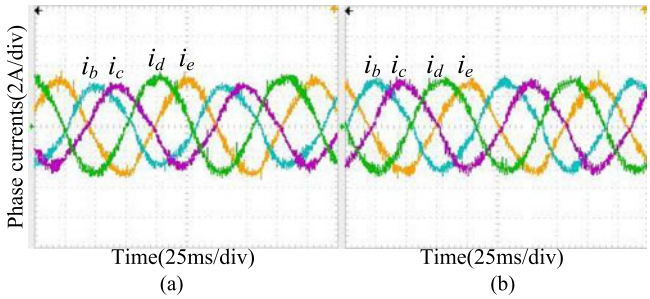

Fig. 8. Healthy phase currents with $i_q = 2\text{A}$ under: (a) LJL criterion. (b) EJL criterion.

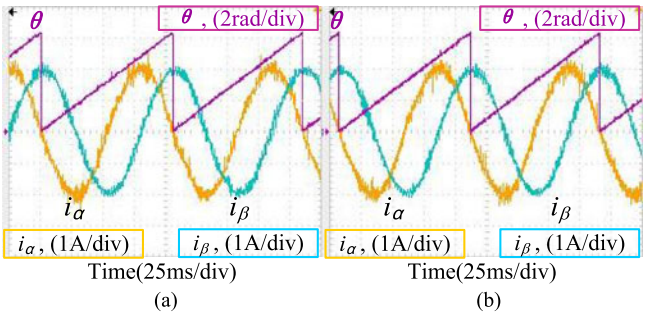

Fig. 9. Waveforms of α–β frame currents and rotor position with $i_q = 2$ A under: (a) LJL control criterion; (b) EJL control criterion.

and 0.48841 N·m, respectively. According to solutions of (36), the fundamental torque is 5.154 N·m, and second and fourth harmonics are 0.2832 and 0.4582 N·m, respectively. The results by FEA also remain close to solutions of (36), and by this the accuracy of proposed model can also be confirmed.

V. EXPERIMENTAL MEASUREMENTS

An experiment set composed of a 5Ph PM motor, a 5Ph half-bridge inverter, and a dc generator as the load has been developed for verification of the suitability of the proposed model and the proposed control algorithm. A 32-bit floating point DSC (TMS320F28335) and a FPGA (XC3S500E) are utilized for the implementation of the overall control algorithm. Fig. 6 shows the control scheme of the 5Ph PM motor for the postfault operation. In the block diagram the CPWM unit and coordinate transformations are calculated in the FPGA, whereas the fault-tolerant control is completed in the DSC. The rotational inertia of this drive is about $0.335\,\text{kg}\cdot\text{m}^2$, the switching frequency of IGBTs is fixed at 10.30 k Hz, sampling frequency of AD converters is set at 5.15 k Hz, and the dc-link voltage is 300 V. The motor structure parameters are shown in Table II also some measured electrical parameters are listed in Table V.

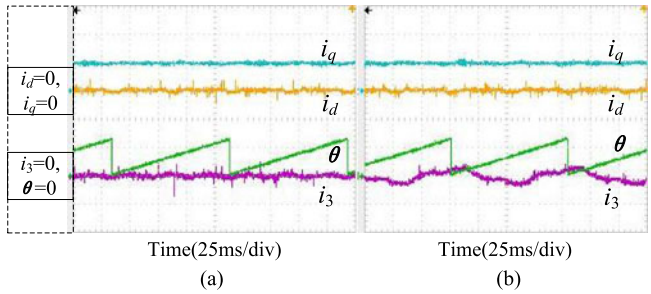

Fig. 10. Waveforms of d–q–3 frame currents and rotor position with $i_q = 2$ A under: (a) LJL criterion; (b) EJL criterion; i_d, i_q, and i_3 are scaled to 2A/div, θ scaled to 4 rad/div.

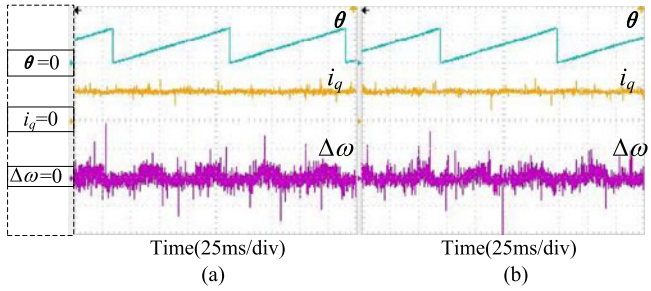

Fig. 11. Waveforms of rotor position, q-axis current and ripple speed with $i_q = 2$ A under: (a) LJL control criterion; (b) EJL control criterion; i_q is scaled to 2 A/div, $\Delta\omega$ is scaled to 10 r/(min·div), θ scaled to 4 rad/div.

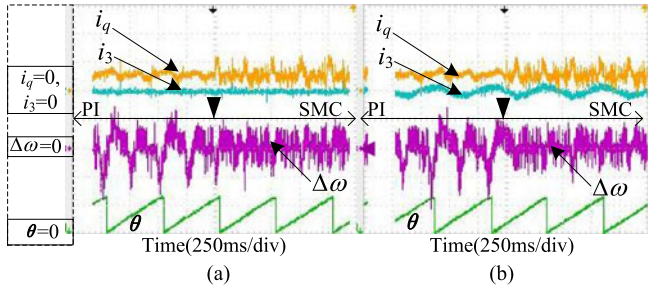

Fig. 12. Waveforms for speed ripples suppression with PI and SMC under: (a) LJL criterion; (b) EJL criterion; i_q and i_3 are scaled to 2 A/div, $\Delta\omega$ is scaled to 5 r/(min·div), θ scaled to 4 rad/div.

A. Implementation of FOC Under Faulty Condition

One should note that oscilloscope used during the experiment has only four input channels, which is the reason why in Fig. 7

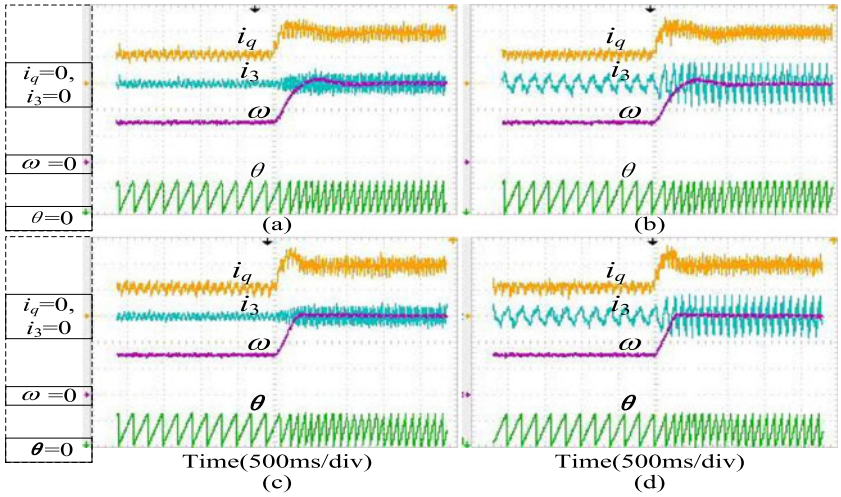

Fig. 13. Speed step response from 150to 300 r/min with a full load under: (a) LJL criterion with PI; (b) EJL criterion with PI; (c) LJL criterion with SMC; (d) EJL criterion with SMC; i_q and i_3 are scaled to 1 A/div, ω is scaled to 100 $\mathrm{r/(min{\cdot}div)}$, θ scaled to 4 rad/div.

only four back-EMFs curves are shown. For the sake of improving iron utilization, a 5Ph PM motor, as shown in Fig. 7, is designed to give a trapezoidal back-EMF. The third harmonics of back-EMFs will cause torque ripples, and this deteriorates the speed performance in the postfault operation.

Fig. 8 refers to healthy phase currents under, respectively, the LJL and EJL control criteria with $i_q = 2$A. In Fig. 8(a), LJL control is performed and the maximum amplitude of remaining phase currents is 2.936 A. In Fig. 8(b), attributed to the EJL control criterion current amplitudes of remaining phases are equal with value of up to 2.76 A. The presented Clarke transformation is not unitary matrix, thus the amplitude of healthy current cannot be kept equal to 2 A. As can be seen from Fig. 8, the postfault control is effective based on proposed model under, respectively, the LJL and EJL criteria.

Fig. 9 shows waveforms of α–β frame currents and rotor position with $i_q = 2$A. As can be seen under the LJL and EJL control criteria, i_α and i_β are orthogonal to each other with equal amplitudes (2 A), and this means that value of fundamental MMF is preserved equal to the healthy case one.

Fig. 10 refers to waveforms of *d*–*q*–3 frame currents and rotor position under the LJL and EJL control criteria. As can be seen, the profiles of i_d and i_q are plane with almost no distortion, and it means a synchronous frame PI controller is effective. Adopting $i_3 = 0$ control under the LJL criteria in Fig. 10(a), $i_3 = 0.236 i_q \cos\theta$ is used in Fig. 10(b) aiming to keep equal current amplitudes of healthy phases. The PI controller at high speeds showed unsatisfactory performance when tracking ac signals in Fig. 10(b), to improve its performance additional resonant control can be used, but this is out of the scope of this study.

Fig. 11 shows waveforms of rotor position, *q*-axis current and speed ripples ($\Delta\omega$) under, respectively, the LJL and EJL control criteria. As can be noted under both two joule losses control criteria, the speed ripples are within ± 6 r/min corresponding to average value of 300 r/min. The speed ripples ($\Delta\omega$) frequency is at twice and four times of the synchronous speed and it is clearly caused by third harmonics of air-gap flux.

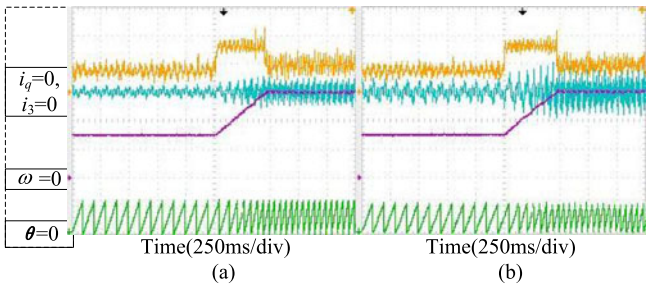

Fig. 14. Speed step response from 300 to 600 r/min with 50% rated load under: (a) LJL criterion with SMC; (b) EJL criterion with SMC; i_q and i_3 are scaled to 1 $\mathrm{A/div}$, ω is scaled to 200 $\mathrm{r/(min{\cdot}div)}$, θ scaled to 4 $\mathrm{rad/div}$.

The ripples in the speed are small, and this can be explained by the fact that torque ripples are filtered by the rotational inertia of the shaft. Hence, a conclusion can be draw that by applying of proposed transformations and current PI controllers at *d*–*q*–3 frame, the output torque ripples are virtually minimal except of some ripples that are caused by third harmonics of air-gap flux.

B. Nonlinear Speed Control Under Faulty Condition

Fig. 12(a) shows the contrast between experiments for speed ripples suppression with PI and SMC. As can be seen from Fig. 12(a), which is under the LJL criterion, the PI controller has speed ripples within ± 7 r/min corresponding to average value of 60 r/min. And then at the instant of 1.25 s SMC is active and speed ripples are restrained to ± 4 r/min. Also comparisons are carried out before and after applying SMC under the ELJ criterion, and similar results are achieved as shown in Fig. 12(b). Those experimental results validate the proposed SMC has a potential of speed ripple suppression.

Fig. 13 shows the speed step response under PI and SMC with a full load. Fig. 13(a) shows the PI controller under the LJL criterion and the speed settle time is within 1 s from 150 to 300 r/min. Fig. 13(c) shows SMC also under the LJL criterion with settle time equal to 0.3 s. As can be seen, in comparison with

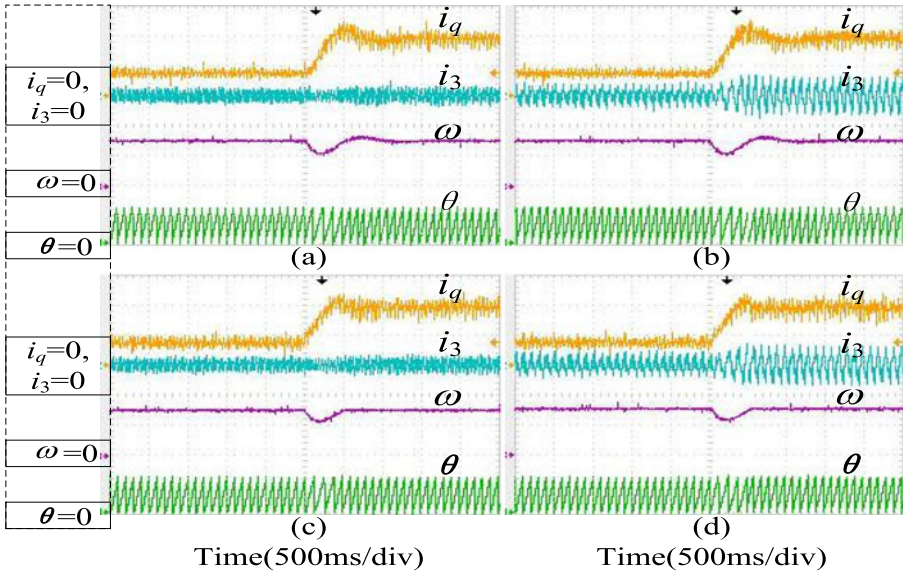

Fig. 15. Motor postfault operation under load disturbance at the instant of 2.5 s, 300 r/min under: (a) LJL criterion with PI; (b) EJL criterion with PI; (c) LJL criterion with SMC; (d) EJL criterion with SMC; i_q and i_3 are scaled to 1 A/div, ω is scaled to 200 r/min, θ scaled to 4 rad/div.

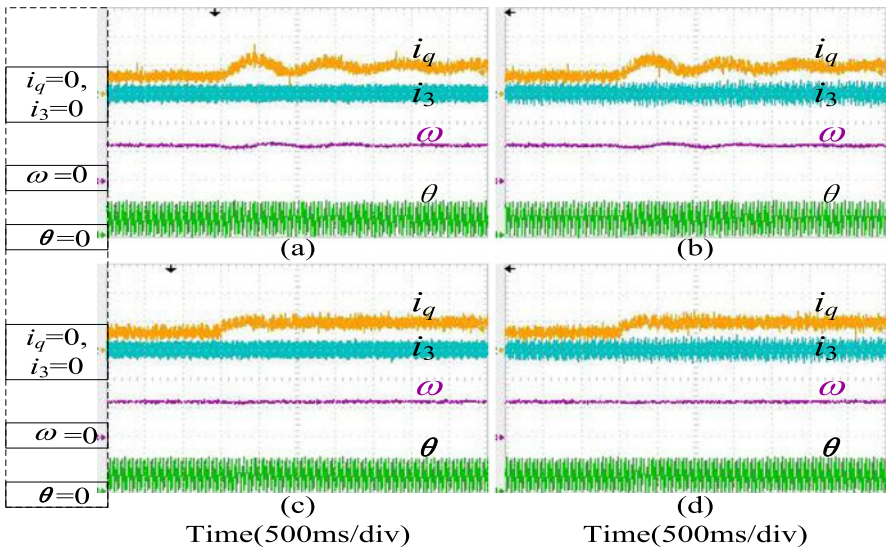

Fig. 16. Motor post-fault operation under load disturbance at the instant of 1.5 s instant, 600 r/min under: (a) LJL criterion with PI; (b) EJL criterion with PI; (c) LJL criterion with SMC; (d) EJL criterion with SMC; i_q and i_3 are scaled to 1 A/div, ω is scaled to 500 r/min, θ scaled to 4 rad/div.

a PI controller [as shown in Fig. 13(a)], the speed response with SMC has no overshoot, and a fast convergence rate is presented. This conclusion is also confirmed by experimentation shown in Fig. 13(b) and (d) under the EJL criterion

Fig. 14 shows the speed step response with 50% rated load. Fig. 14(a) refers to the speed step response with SMC under the LJL criterion and the speed settle time is 0.5 s from 300 to 600 r/min (rated speed). Fig. 14(b) exhibits the speed step response under the EJL criterion and the settle time is also 0.5 s. The speed response has no overshoot and a good steady behavior is always achievable.

Fig. 15 demonstrates the motor postfault operation with a full load at 300 r/min. Fig. 15(a) and (c) shows motor operated under the LJL criterion with PI and SMC, respectively. As can be noted after the occurrence of a disturbance in the load, speed settle time is about 1 s with PI controller whereas with SMC this time is 0.5 s, which is nearly half of the settle time with a PI controller. Similar results can be obtained when the motor is operated with the EJL criterion, as shown in Fig. 15(b) and (d).

Fig. 16 shows the motor postfault operation with 25% of rated load disturbance applied at 600 r/min. Fig. 16(a) and (c) refers to the LJL control criterion with PI and SMC, respectively. As can be seen with a PI controller, there are noticeable speed oscillations and the settle time is 2 s long, whereas with SMC oscillations in the speed response are absent. The motor operation under the EJL control criterion yields similar

performance as shown in Fig. 16(b) and (d). Consequently, with SMC the speed behavior in the presence of disturbance in the load is found to be satisfactory.

VI. Conclusion

This paper proposes a decoupled modeling of the 5Ph PM motor under single-phase open fault. Based on this model, the postfault control can be done with the FOC method. This model is based on concepts of preserving the postfault value of both fundamental MMF and back-EMFs equal to the normal operation, thus electromagnetic energy conversion can be sustainable. However, due to incapability of preserving MMF and back-EMFs of third space, the torque behavior is fluctuated. To suppress these fluctuations and improve speed performance, SMC in the speed loop is proposed.

The proposed model is verified by FEA under the LJL and EJL control criteria, and results show that the spectrum of output torque is consistent with the proposed analytical model.

Experiments were carried out on a 5Ph drive to verify the proposed control technique and the postfault motor model. FOC of the motor with an *A*-phase open circuit was performed, and plain *d*–*q* frame current profile was achieved. Proposed SMC in the speed loop was utilized and as a result the waveform of rotor speed became steady, which stand as a confirmation of successful speed ripples suppression. Along with that, fast convergence and small static error in the speed response were achieved.

In its structure proposed SMC contains a PI controller and a chattering term (shown as a saturation function or a sign function), which makes it easy to implement in a DSC without long computational process.

References

[1] P. Garg, S. Essakiappan, H. S. Krishnamoorthy, and P. N. Enjeti, "A fault-tolerant three-phase adjustable speed drive topology with active common-mode voltage suppression," *IEEE Trans. Power Electron.*, vol. 30, no. 5, pp. 2828–2839, May 2015.

[2] Y. Hu, C. Gan, W. Cao, J. Zhang, W. Li, and S. J. Finney, "Flexible fault-tolerant topology for switched reluctance motor drives," *IEEE Trans. Power Electron.*, vol. 31, no. 6, pp. 4654–4668, Jun. 2016.

[3] M. Salehifar, R. S. Arashloo, J. M. Moreno-Equilaz, V. Sala, and L. Romeral, "Fault detection and fault tolerant operation of a five phase PM motor drive using adaptive model identification approach," *IEEE J. Emerg. Sel. Topics Power Electron.*, vol. 2, no. 2, pp. 212–223, Jun. 2014.

[4] M. I. Masoud, S. M. Dabour, A. E. W. Hassan, and E. M. Rashad, "Control of five-phase induction motor under open-circuit phase fault fed by fault tolerant VSI," in *Proc. IEEE 10th Int. Symp. Diagnostics Elect. Mach., Power Electron. Drives*, 2015, pp. 327–332.

[5] A. S. Abdel-Khalik, M. A. Elgenedy, S. Ahmed, and A. M. Massoud, "An improved fault-tolerant five-phase induction machine using a combined star/pentagon single layer stator winding connection," *IEEE Trans. Ind. Electron.*, vol. 63, no. 1, pp. 618–628, Jan. 2016.

[6] M. Jones, S. N. Vukosavic, D. Dujic, and E. Levi, "A synchronous current control scheme for multiphase induction motor drives," *IEEE Trans. Energy Convers.*, vol. 24, no. 4, pp. 860–868, Dec. 2009.

[7] H. Guzman *et al.*, "Comparative study of predictive and resonant controllers in fault-tolerant five-phase induction motor drives," *IEEE Trans. Ind. Electron.*, vol. 63, no. 1, pp. 606–617, Jan. 2016.

[8] G. Liu, L. Qu, W. Zhao, Q. Chen, and Y. Xie, "Comparison of Two SVPWM control strategies of five-phase fault-tolerant permanent-magnet motor," *IEEE Trans. Power Electron.*, vol. 31, no. 9, pp. 6621–6630, Sep. 2016.

[9] S. K. Barik and K. K. Jaladi, "A comparative analysis of different conduction modes in VSI with five phase induction motor," in *Proc. 2016 Int. Conf. Microelectron., Comput. Commun.*, 2016, pp. 1–6.

[10] S. Dwari and L. Parsa, "Fault-tolerant control of five-phase permanent-magnet motors with trapezoidal back EMF," *IEEE Trans. Ind. Electron.*, vol. 58, no. 2, pp. 476–485, Feb. 2011.

[11] A. Mohammadpour and L. Parsa, "A unified fault-tolerant current control approach for five-phase pm motors with trapezoidal back EMF under different stator winding connections," *IEEE Trans. Power Electron.*, vol. 28, no. 7, pp. 3517–3527, Jul. 2013.

[12] A. K. M. Arafat and C. Seungdeog, "Fault tolerant control of five-phase permanent magnet assisted synchronous reluctance motor based on dynamic current phase advance," in *Proc. IEEE Energy Convers. Congr. Expo.*, 2015, pp. 1208–1214.

[13] X. Kestelyn and E. Semail, "A vectorial approach for generation of optimal current references for multiphase permanent-magnet synchronous machines in real time," *IEEE Trans. Ind. Electron.*, vol. 58, no. 11, pp. 5057–5065, Nov. 2011.

[14] A. Mohammadpour and L. Parsa, "Global fault-tolerant control technique for multiphase permanent-magnet machines," *IEEE Trans. Ind. Appl.*, vol. 51, no. 1, pp. 178–186, Jan./Feb. 2015.

[15] A. Mohammadpour, S. Sadeghi, and L. Parsa, "A generalized fault-tolerant control strategy for five-phase pm motor drives considering star, pentagon, and pentacle connections of stator windings," *IEEE Trans. Ind. Electron.*, vol. 61, no. 1, pp. 63–75, Jan. 2014.

[16] F. De Belie, X. Kestelyn, and N. K. Nguyen, "Fault-tolerant optimal-current torque-controlled five-phase pmsms with open-circuited phases: Position self-sensing operation," in *Proc. IEEE Vehicle Power Propulsion Conf.*, 2014, pp. 1–6.

[17] R. Hyung-Min, K. Ji-Woong, and S. Seung-Ki, "Synchronous-frame current control of multiphase synchronous motor under asymmetric fault condition due to open phases," *IEEE Trans. Ind. Appl.*, vol. 42, no. 4, pp. 1062–1070, Jul./Aug. 2006.

[18] H. A. Toliyat, S. P. Waikar, and T. A. Lipo, "Analysis and simulation of five-phase synchronous reluctance machines including third harmonic of airgap MMF," *IEEE Trans. Ind. Appl.*, vol. 34, no. 2, pp. 332–339, Mar./Apr. 1998.

[19] M. A. Fnaiech, F. Betin, G. A. Capolino, and F. Fnaiech, "Fuzzy logic and sliding-mode controls applied to six-phase induction machine with open phases," *IEEE Trans. Ind. Electron.*, vol. 57, no. 1, pp. 354–364, Jan. 2010.

[20] L. Faa-Jeng, H. Ying-Chih, and T. Meng-Ting, "Fault-tolerant control for six-phase PMSM drive system via intelligent complementary sliding-mode control using TSKFNN-AMF," *IEEE Trans. Ind. Electron.*, vol. 60, no. 12, pp. 5747–5762, Dec. 2013.

[21] M. A. Elgenedy, A. S. Abdel-Khalik, A. Elserougi, S. Ahmed, and A. Massoud, "Fault-tolerant control of five-phase current source inverter for medium-voltage drives," in *Proc. 7th IET Int. Conf. Power Electron., Mach. Drives*, 2014, pp. 1–6.

[22] A. Mohammadpour, S. Mishra, and L. Parsa, "Fault-tolerant operation of multiphase permanent-magnet machines using iterative learning control," *IEEE J. Emerg. Sel. Topics Power Electron.*, vol. 2, no. 2, pp. 201–211, Jun. 2014.

[23] H. H. Choi, N. T. T. Vu, and J. W. Jung, "Digital implementation of an adaptive speed regulator for a PMSM," *IEEE Trans. Power Electron.*, vol. 26, no. 1, pp. 3–8, Jan. 2011.

[24] G. H. B. Foo and M. F. Rahman, "Direct torque control of an IPM-synchronous motor drive at very low speed using a sliding-mode stator flux observer," *IEEE Trans. Power Electron.*, vol. 25, no. 4, pp. 933–942, Apr. 2010.

[25] V. I. Utkin, "Sliding mode control in dynamic systems," in *Proc. 32nd IEEE Conf. Decision Control, 1993.*, 1993, pp. 2446–2451.

[26] D. Swaroop, J. K. Hedrick, P. P. Yip, and J. C. Gerdes, "Dynamic surface control for a class of nonlinear systems," *IEEE Trans. Autom. Control*, vol. 45, no. 10, pp. 1893–1899, Nov. 2000.

[27] R. M. T. R. Ismail, N. D. That, and Q. P. Ha, "Adaptive fuzzy sliding mode control for uncertain nonlinear underactuated mechanical systems," in *Proc.Int. Conf. Control, Autom. Inf. Sci.*, 2013, pp. 212–217.

[28] M. Choux, H. R. Karimi, G. Hovland, M. R. Hansen, M. Ottestad, and M. Blanke, "Robust adaptive backstepping control design for a nonlinear hydraulic-mechanical system," in *Proc. 48th Conf. Decision Control, 2009 Held Jointly With 2009 28th Chin. Control Conf.*, 2009, pp. 2460–2467.

[29] F. J. Lin, C. K. Chang, and P. K. Huang, "FPGA-based adaptive backstepping sliding-mode control for linear induction motor drive," *IEEE Trans. Power Electron.*, vol. 22, no. 4, pp. 1222–1231, Jul. 2007.

[30] X. Zhang, L. Sun, K. Zhao, and L. Sun, "Nonlinear speed control for PMSM system using sliding-mode control and disturbance compensation techniques," *IEEE Trans. Power Electron.*, vol. 28, no. 3, pp. 1358–1365, Mar. 2013.
[31] W. Wei, C. Ming, Z. Bangfu, Z. Ying, and D. Shichuan, "A fault-tolerant permanent-magnet traction module for subway applications," *IEEE Trans. Power Electron.*, vol. 29, no. 4, pp. 1646–1658, Apr. 2014.
[32] T. Wang, H. Xu, J. Han, E. Elbouchikhi, and M. E. H. Benbouzid, "Cascaded H-bridge multilevel inverter system fault diagnosis using a PCA and multiclass relevance vector machine approach," *IEEE Trans. Power Electron.*, vol. 30, no. 12, pp. 7006–7018, Dec. 2015.
[33] R. Hyung-Min, K. Ji-Woong, and S. Seung-Ki, "Synchronous frame current control of multi-phase synchronous motor. Part I. Modeling and current control based on multiple d-q spaces concept under balanced condition," in *Proc. 39th IAS Annu. Meeing. Conf. Rec. 2004 IEEE Ind. Appl. Conf.*, pp. 56–63, 2004.
[34] L. Parsa and H. A. Toliyat, "Fault-tolerant interior-permanent-magnet machines for hybrid electric vehicle applications," *IEEE Trans. Veh. Technol.*, vol. 56, no. 4, pp. 1546–1552, Jul. 2007.

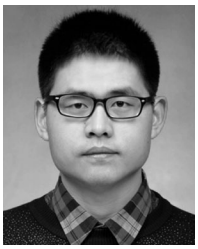

Bing Tian received the B.S. and M.S. degrees in electrical engineering from Harbin Engineering University, Harbin, China, in 2011 and 2013, respectively. He is currently working toward the Ph.D. degree in electrical engineering at Harbin Institute of Technology.

His research interests include PM electric machines and drives, and renewable energy.

Qun-Tao An (S'10–M'11) received the B.S. degree in electrical engineering from Harbin University of Science and Technology, Harbin, China, in 2004, and the M.S. and Ph.D. degrees in electrical engineering from Harbin Institute of Technology, Harbin, China, in 2006 and 2011, respectively.

From 2009 to 2010, he was an honorary Fellow at Wisconsin Electric Machines and Power Electronics Consortium, University of Wisconsin-Madison, Madison, WI, USA. From 2009, he joined the Faculty of Harbin Institute of Technology, and he is currently an Associate Professor. His research interests include electric machines and drives, power electronics, and energy storage technology.

Jian-Dong Duan received the B.S. degree from Northeast Forestry University, Harbin, China, in 2007, the M.S. and Ph.D. degrees in electrical engineering from Harbin Institute of Technology, Harbin, China, in 2009 and 2014, respectively.

He is currently with the Department of Electrical Engineering, Harbin institute of technology. His research interests include renewable energy and motor drive.

Dong-Yang Sun received the B.S. and M.S. degrees in electrical engineering from Harbin University of Science and Technology, Harbin, China, in 2011 and 2014, respectively. He is currently working toward the Ph.D. degree in electrical engineering at Harbin Institute of Technology.

His research interests include wind power technology, and electric machines and drives.

Li Sun (M'08) received the B.S., M.S., and Ph.D. degrees in electrical engineering from Harbin Institute of Technology, Harbin, China, in 1982, 1986, and 1991, respectively.

Since 1986, he has been with the Department of Electrical Engineering, Harbin Institute of Technology, where he is currently a Professor of electrical engineering. His research interests include electric machines and drives, renewable energy, power electronics, and EMC.

Dmitry Semenov received the B.S. degree in power engineering from Ural Federal University, Yekaterinburg, Russia, in 2014. He is currently working toward the M.S. degree in electrical engineering at Harbin Institute of Technology, Harbin, China.

His research interests include industrial automation, and electric machines and drive